



doi 10.26089/NumMet.v25r210

## Numerical image denoising and deblurring via an approximate weighted mean curvature flow model

Alexandre Timonov

St. Petersburg Department of V. A. Steklov Institute of Mathematics of the Russian Academy of Sciences,  
St. Petersburg, Russia

University of South Carolina Upstate, Spartanburg, USA

ORCID: 0009-0009-0530-9721, e-mail: [altim@pdmi.ras.ru](mailto:altim@pdmi.ras.ru)

**Abstract:** A new mathematical model for image denoising and deblurring is proposed and numerically implemented. It is based on a geometric differential equation that describes motion of a level surface of its solution by the weighted mean curvature. The numerical experiments are carried out to demonstrate the computational effectiveness of the proposed technique in comparison with the weighted total variation flow and VH-regularization.

**Keywords:** denoising and deblurring, total variation, weighted mean curvature, geometric equation, numerical experiments.

**For citation:** A. Timonov, “Numerical image denoising and deblurring via an approximate weighted mean curvature flow model,” *Numerical Methods and Programming*. 25 (2), 115–126 (2024). doi 10.26089/NumMet.v25r210.

## Численное устранение шума и нечеткости изображений с помощью приближенной модели движения под влиянием средней кривизны с весом

Александр А. Тимонов

Санкт-Петербургское отделение Математического института имени В. А. Стеклова РАН,  
Санкт-Петербург, Россия

Университет штата Южная Каролина Апстейт, Спартанбург, США

ORCID: 0009-0009-0530-9721, e-mail: [altim@pdmi.ras.ru](mailto:altim@pdmi.ras.ru)

**Аннотация:** Предложена и численно реализована новая математическая модель устранения шума и нечеткости изображений. Она основана на геометрическом дифференциальном уравнении, которое описывает движение поверхности уровня его решения под влиянием средней кривизны с весом. Численные эксперименты проводятся с целью демонстрации вычислительной эффективности предлагаемого метода в сравнении с методом полной вариации с весом и VH-регуляризацией.

**Ключевые слова:** устранение шума и нечеткости изображений, полная вариация, средняя кривизна, геометрическое уравнение, численные эксперименты.

**Для цитирования:** Тимонов А.А. “Численное устранение шума и нечеткости изображений с помощью приближенной модели движения под влиянием средней кривизны с весом,” // *Вычислительные методы и программирование*. 2024. 25, № 2. 115–126. doi 10.26089/NumMet.v25r210.



**1. Introduction.** In this paper the problem of image denoising and deblurring is revisited. The actual and potential applications of image denoising and deblurring to many areas of science and technology, especially to geophysics and medical diagnostics, are numerous. As an example, we refer to a relatively new medical diagnostic modality, cardiac CT [1]. As early as 2014, the invention of the dual-source multi-slice computed tomography gave rise to an alternative to the conventional invasive cardiac angiography and, in essence, led to emerging into medical diagnostics a new imaging modality, the Electron Beam Computer Tomograph (EBCT) (see, e.g., [2]) that has no moving parts. This allowed for increasing the temporal resolution and, as a result, to overcome the low heartbeat requirement and reduce the contrast media administration. However, despite the significant progress in cardiac CT, the conventional heart angiography is still advantageous, especially for planning surgeries. Indeed, the temporal resolution of the latter is about 10–15 ms, whereas it is 65–75 ms for a cardiac CT. The spatial resolution of the conventional angiography is 0.1–0.2 mm, while it is about 0.3–0.5 mm in a cardiac CT. As a consequence, the reconstructed images are usually more noisy and blurred. Thus, the problem of image denoising and deblurring remains one of the top priorities for the cardiac CT imaging modalities. The main challenge is to enhance significantly their temporal and spatial resolutions.

In this paper a data-driven model of an observed image  $\tilde{v}$  is utilized

$$\tilde{v} = Av + \mathcal{N},$$

where  $A : L^2(\Omega) \rightarrow L^2(\Omega)$  is a linear bounded operator,  $v$  is the ground truth image, and  $\mathcal{N}$  is a random noise. Here,  $\Omega \subset \mathbb{R}^2$  is supposed to be a bounded connected domain with the Lipschitz boundary  $\partial\Omega$ . The problem is as follows: given the triple  $(A, \tilde{v}, \mathcal{N})$ , find some approximations of  $v$ . Clearly, if  $A = I$ , then the problem represents image denoising. If  $A$  is a linear integral operator with a  $L^2$ -kernel, then image deblurring takes place. If  $A$  (or  $A^*A$ ) is not invertible or an inverse of  $A$  is not continuous, then the problem is ill-posed in the sense of Hadamard. Therefore, it is natural to use Tikhonov regularization, i.e., to minimize a functional

$$T_\alpha(v) = \|Av - \tilde{v}\|_{L^2(\Omega)}^2 + \alpha S(v), \tag{1}$$

where  $\alpha = \text{const} > 0$  is the regularization parameter, and  $S$  is a stabilizer. However, it is well known that if  $S(v) = \|v\|_{L^2}^2$ , then a reconstructed image is not regular, and if  $S(v) = \|v\|_{H^1}^2$ , then too much regularity is imposed. In both cases, obtaining high-resolution images is highly problematic.

To overcome these drawbacks, the idea of utilizing the one dimensional Arzela variation as  $S$  was pioneered in [3–5]. Later, the total Vitalli and Hardi variations were exploited in two dimensions in [6]. In [7], the Phillips’ (residual) method [8] was applied to obtain sought approximations. As follows from [9], this method is equivalent to the unconstrained problem of minimizing (1), where the stabilizer was chosen to be the total variation defined by Giusti [10]. Introducing the space of functions of bounded variation (BV-space) is associated with the fact that this functional may have no minimizers in the non-reflexive Banach space  $W^{1,1}(\Omega)$ . Moreover, the BV-space is a natural framework for image processing since it allows for edges, i.e., the curves in an image along which  $\nabla v$  is large. The following question arises about constructing a minimizing sequence for (1). Since  $T_\alpha(v)$  is not differentiable, it may seem that a subgradient method may be used for this purpose. However, it is not a descent method, which means that the values of  $T_\alpha$  may increase. Also, the convergence of any subgradient method is much more slower than a Newton-like method. Therefore, even leaving aside the difficulties in the numerical implementation of a subgradient method, it is used in computations only in combination with the primal or dual decomposition techniques (see, e.g., [11]). Moreover, these combinations suffer from the so-called staircase phenomenon, which means that they tend to create constant patches in a reconstructed image. As it was observed and proved in [12], the structure of these approximations is such that in two dimensions their gradients are parallel to one of the coordinate axes. The similar results were obtained in [13] for a discrete analogue of the Tikhonov functional. In addition, a loss of contrast in the restored images was also observed.

This is what motivated the interest in the PDF-based methods which are free from the need to compute the subgradient of  $T_\alpha(v)$ . All such methods utilize an Euler–Lagrange equation for  $T_\alpha$ . For  $S(v) = \int_\Omega |\nabla v| dx, v \in C^1(\Omega), |\nabla v| > 0$  the Euler–Lagrange equation is formally derived as

$$-2A^*(Au - \tilde{v}) + \alpha \nabla \cdot \left( \frac{\nabla u}{|\nabla u|} \right) = 0. \tag{2}$$

A fairly large number of models based on the Euler–Lagrange equation are available in the mathematics literature. They are referred to as the total variation flow models. In [14] it was proposed a general approach



to constructing such models. As an example, we indicate a total variation flow model associated with (2) and represented by the evolution problem

$$u_t = \alpha \nabla \cdot \left( \frac{\nabla u}{|\nabla u|} \right) - 2A^*(Au - \tilde{v}) \quad \text{in } \Omega \times (0, \infty), \tag{3}$$

$$\nabla u \cdot \nu = 0 \quad \text{on } \partial\Omega \times (0, \infty), \tag{4}$$

$$u(\cdot, 0) = \tilde{v} \quad \text{in } \bar{\Omega} \times \{0\}, \tag{5}$$

where  $\nu$  is the outward normal to  $\partial\Omega$ . It is well known (see, e.g., [14]) that under certain conditions, the equilibrium solutions of (3)–(5) approximate the minimizers of (1), so that the staircase effect is suppressed, sometimes significantly, and the loss of contrast is compensated but often incompletely and not in all cases.

To expand the scope of effective applications of PDF-based models to image denoising and deblurring, we propose to utilize properties of a geometric equation  $u_t + F(\nabla u, \nabla^2 u) = 0$ , i.e., an evolution equation for the level surface of  $u$  [15, 16]. Within the framework of the example indicated above, a geometric equation is given by

$$u_t = |\nabla u| \left[ \alpha \nabla \cdot \left( \frac{\nabla u}{|\nabla u|} \right) - 2A^*(Au - \tilde{v}) \right]. \tag{6}$$

Here,  $u_t/|\nabla u|$  is the normal speed of the level surface of  $u$ , and  $H = \nabla \cdot (\nabla u/|\nabla u|)$  is the mean curvature of this surface. This equation describes motion of the level surface of  $u$  by its mean curvature at every point where  $|\nabla u| \neq 0$ . The term  $|\nabla u|H$  diffuses in the direction orthogonal to  $\nabla u$  while it does not diffuse in the direction of  $\nabla u$ . This allows for smoothing  $u$  outside of an edge with almost no smoothing on the edge. However, the differential operator in the right-hand side of (6) is, in general, singular and elliptic degenerate at all points where  $|\nabla u| = 0$ . Although the viscosity theory may be used by analogy with [15–17] for establishing existence of the weak solutions to (6) subject to (4) and (5), it cannot be used in computations due to the absence of uniqueness and stability.

Based on a geometric equation, we propose an approximate weighted mean curvature flow model for image denoising and deblurring. Specifically, the term  $|\nabla u|$  is regularized in the sense of Evans-Spruck [16], e.i., it is replaced to  $\sqrt{\varepsilon^2 + |\nabla u|^2}$ , and a viscosity term  $\sigma \Delta u$ ,  $\sigma = \text{const} > 0$  [18] is added to the right-hand side of (6). To provide the adaptive diffusivity, we also introduce a weighted mean curvature  $H_\alpha = \nabla \cdot (\alpha(x)\nabla u/|\nabla u|)$ , in which a weight function  $\alpha$  can be viewed as a variable regularization parameter. From a computational point of view, the novelty of the proposed approach lies primarily in the fact that the originally singular and parabolic degenerate geometric equation is approximated by a family of the parametric regular problems that have the classical solutions. In this regard, the central question is: Does a sequence of the parametric solutions converge to the ground truth image as  $t \rightarrow \infty$  and  $\varepsilon, \sigma \rightarrow 0$ ? However, due to the complexity and tedium of analysis of the convergence of approximate solutions, in this paper we aim to studying their numerical convergence. The latter is understood in the sense that if the grid becomes finer and finer then the numerical solution is closer and closer to a certain grid function that is in proximity of the ground truth image. So, in this paper the numerical study is carried out as a useful indication of what one should focus on to prove.

The paper is organized as follows. In the section 2 we formulate the approximate weighted mean curvature flow model for image denoising and deblurring. Its discrete analogue is described in the section 3. Some results of the numerical experiments are presented in the section 4, and the investigation is concluded in the section 5.

**2. An approximate weighted mean curvature flow model.** Let  $\Omega \subset \mathbb{R}^2$  be a bounded connected domain with the Lipschitz boundary  $\partial\Omega$ ,  $v \in L^1(\Omega)$ , and  $\alpha \in C^1(\Omega)$ ,  $\alpha > 0$ . By analogy with [10] we define the weighted total variation of  $v$  as

$$TV_\alpha(v) = \int_\Omega \alpha |Dv| = \sup \left\{ \int_\Omega v \nabla \cdot (\alpha \varphi) dx : \varphi \in C_c^1(\Omega; \mathbb{R}^2), \|\varphi\|_{L^\infty} \leq 1 \right\},$$

where  $\varphi = (\varphi_1, \varphi_2)$  is a vector-valued function, and  $Dv$  is the distributional derivative. To ensure that  $TV_\alpha(v) < \infty$ , assume that  $|Dv|$  is a finite Radon measure in  $\Omega$ . The set  $BV_\alpha(\Omega) = \{v \in L^1(\Omega) : TV_\alpha(v) < \infty\}$  endowed with the norm

$$\|v\|_{BV_\alpha(\Omega)} = \|v\|_{L^1(\Omega)} + TV_\alpha(v),$$

is said to be the  $\alpha$ -BV space of functions. Clearly,  $BV_\alpha(\Omega)$  is a Banach space, and the following embedding takes place in two dimensions

$$W^{1,1}(\Omega) \subset BV_\alpha(\Omega) \subset L^2(\Omega).$$

Recall that if  $v \in C^1(\Omega)$  (or  $v \in W^{1,1}(\Omega)$ ), then the definition of  $TV_\alpha$  can be simplified to

$$TV_\alpha(v) = \int_{\Omega} \alpha(x)|\nabla v|dx,$$

and the weight function  $\alpha$  can be viewed as the variable regularization parameter. Following the arguments from [10], one may establish that the functional  $TV_\alpha$  is lower semi-continuous in  $\Omega$ .

By analogy with [19], we represent the Tikhonov functional in the form

$$T_{\alpha\beta}(v) = \|Av - \tilde{v}\|_{L^2(\Omega)}^2 + \beta\|v\|_{L^2(\Omega)}^2 + TV_\alpha(v), \quad \beta = \text{const} \geq 0. \tag{7}$$

Recall that the second term in  $T_{\alpha\beta}$  is introduced to ensure its coercivity for  $\beta > 0$ . Taking into account this property and using the standard technique from the theory of linear ill-posed problems (see, e.g., [9]), by analogy with [19] one may establish the existence of a unique solution to the variational problem

$$\arg \inf \{T_{\alpha\beta}(v) : v \in \mathcal{M} \subset BV_\alpha(\Omega) \cap L^2(\Omega), \beta > 0\}, \tag{8}$$

where  $\mathcal{M}$  is a bounded, closed and convex set in  $L^2(\Omega)$ . Denote its solution as  $v_{\alpha\beta}$ . It is well known that if  $\beta = \alpha = \gamma = \text{const} > 0$  and  $\gamma = \gamma(\delta) : \gamma(\delta) \rightarrow 0$  and  $\delta^2/\gamma(\delta) \rightarrow 0$  as  $\delta \rightarrow 0$ , then according to [9]  $v_{\gamma(\delta)} \rightarrow v$  as  $\delta \rightarrow 0$  in  $L^2(\Omega)$ . Obviously, any function  $\gamma(\delta) = C\delta^q$ ,  $1 < q < 2$ , where  $C > 0$  is a real number, satisfies these asymptotic conditions. However, in practice the noise level  $\delta$  is always fixed, so that  $\gamma$  is fixed as well. Under this condition, one can only hope that some approximations  $v_\gamma$  would be close enough to the ground truth image  $v$ . In image processing the parameters  $C$  and  $q$  are often selected by trials. This technique may be successful, especially for structurally simple images. If an image contains a variety of edges, i.e., curves on which the intensity has removable discontinuities, then introducing a weight function  $\alpha$  becomes necessary in order to provide the restoration of the high resolution images. However, the problem of constructing an effective weight function remains open.

Now, we assume that the weight function  $\alpha$  is positive, sufficiently smooth (e.g.,  $\alpha \in C^{1,1}(\Omega)$  (see [20] for detail)) and bounded away from zero and infinity and introduce the differential operator

$$H_\alpha(\nabla u) = \nabla \cdot \left( \alpha \frac{\nabla u}{|\nabla u|} \right) \tag{9}$$

at points in  $\Omega$  where  $|\nabla u| > 0$ . Also, we assume that it is positive on  $\partial\Omega$ . By analogy with [17] we introduce a nonlinear initial boundary value problem for a geometric equation, which is associated with the variational problem (8)

$$u_t = |\nabla u| \left[ \nabla \cdot \left( \alpha(x) \frac{\nabla u}{|\nabla u|} \right) - A^*(Au - \tilde{v}) \right] \quad \text{in } \Omega \times (0, \infty), \tag{10}$$

$$\nabla u \cdot \nu = 0 \quad \text{on } \partial\Omega \times (0, \infty), \tag{11}$$

$$u(\cdot, 0) = \tilde{v} \quad \text{in } \bar{\Omega} \times \{0\}. \tag{12}$$

Clearly, the operator (9) represents the weighted mean curvature defined at every point of the level surface of  $u$  where  $|\nabla u| > 0$ . It should be mentioned that the parameter  $\beta$  is set to zero in the Euler–Lagrange equation for (7) since there is no longer a need to minimize the latter. The homogeneous Neumann boundary condition is imposed to prevent the flow flux across  $\partial\Omega$ , which is usually done in image processing. Thus, the equation (10) is as a geometric equation which governs moving the level surface of  $u$  with the normal speed  $u_t/|\nabla u|$  by its weighted mean curvature.

In general, the nonlinear operator (9) is singular and elliptic degenerate. This circumstance significantly complicates the analysis of the conditions for the unique solvability of (10)–(12) and its stability. Although existence of a weak viscosity solution to (10)–(12) may be established by analogy with [17], it was shown there that even for  $\alpha = 1$  and the Dirichlet boundary condition there exists a collection of equilibria for the flow (10)–(12). Moreover, to the best of the author’s knowledge, there are no results published in the mathematics literature



on the stability of this or similar problems. Thus, there is no reason to believe that (10)–(12) is well-posed in the sense of Hadamard. This means that such a problem cannot be used, at least directly, as a computational model. To make (10)–(12) suitable for the computational implementation, we make approximations following Evans-Spruck [16] and Temam-Lichniewsky [18]. Specifically, the term  $|\nabla u|$  is approximated by the  $\varepsilon$ -parametric functions  $g_\varepsilon(p) = (\varepsilon^2 + p^2)^{1/2}$ ,  $\varepsilon > 0$ ,  $p = |\nabla u|$ , and the elliptic degeneracy of  $H_w(\nabla u)$  is treated by adding the viscosity term  $\sigma \Delta u$ ,  $0 < \sigma < 1$ . As a result, we obtain the approximate weighted mean curvature flow model

$$u_t^{(\sigma\varepsilon)} = g_\varepsilon(|\nabla u^{(\sigma\varepsilon)}|) \nabla \cdot \left[ a(x, |\nabla u^{(\sigma\varepsilon)}|) \nabla u^{(\sigma\varepsilon)} - A^*(Au - v_m) \right] \quad \text{in } Q_T, \tag{13}$$

$$\nabla u^{(\sigma\varepsilon)} \cdot \nu = 0 \quad \text{on } \partial\Omega \times (0, T], \tag{14}$$

$$u^{(\sigma\varepsilon)}(x, 0) = v_m(x) \quad \text{in } \bar{\Omega} \times \{0\}, \tag{15}$$

where

$$a(x, p) = \frac{\alpha(x)}{g_\varepsilon(p)} + \sigma, \quad p = |\nabla u^{(\sigma\varepsilon)}|.$$

Here,  $Q_T = \Omega \times (0, T)$ ,  $T > 0$ , and  $v_m$  is a mollification of  $\tilde{v}$ , i.e.,  $v_m = m * \tilde{u}$ ,  $m$  is a mollifier. It is well known (see, e.g., [21]) that for sufficiently smooth  $\bar{\Omega}$  and  $\alpha$  one may ensure existence of a unique classical solution  $u^{(\sigma\varepsilon)} \in C^{2+\nu, 1+\nu/2}(Q_T)$ . Moreover,  $\|u\|_{C^{2+\nu, 1+\nu/2}(Q_T)} \leq C \|\tilde{u}\|_{C^{2,\nu}(\Omega)}$ , where  $C = \text{const} > 0$  that does not depend on  $t$ . Under these conditions, the approximate problem (13)–(15) is well-posed. This opens the door for applying the efficient finite-difference methods to the numerical solution of (13)–(15). The central question is about the proximity of approximations  $u^{(\sigma\varepsilon)}$  to the ground truth image  $v$  at sufficiently large  $T$  and sufficiently small  $\sigma, \varepsilon$ .

**3. Discretization.** We first apply the Rothe method [22] to (13)–(15). This choice is motivated by the fact of using this method by Ladyzhenskaya [23] and Ventzel [24] for establishing the existence and uniqueness results for quasi-linear parabolic equations. According to the Rothe’s method, we intersect the cylinder  $Q_T$  by hyperplanes  $t_k = k\tau$ ,  $\tau = T/K$ , ( $k = 0, 1, \dots, K$ ), and let  $\Omega_k$  be its  $k$ th cross section. For each  $t = t_k$  we approximate the temporal derivative  $u_t$  by the backward difference formula

$$u_t^{(\sigma\varepsilon)}(x, t_k) \approx \frac{w^{(k)}(x) - w^{(k-1)}(x)}{\tau},$$

where  $w^{(k)}(x) = w(x, t_k)$  satisfies the linear elliptic boundary value problem

$$\frac{w^{(k)}(x) - w^{(k-1)}(x)}{\tau} = g_\varepsilon(|\nabla w^{(k-1)}|) \left[ \nabla \cdot \left( a(x, |\nabla w^{(k-1)}|) \nabla w^{(k)} \right) - A^*(Aw^{k-1} - v_m) \right] \quad \text{in } \Omega_k, \tag{16}$$

$$\nabla w^{(k)} \cdot \nu = 0 \quad \text{on } \partial\Omega_k, \tag{17}$$

where  $w^0 = v_m$  in  $\Omega_0$ . Solving this problem for any fixed integer  $K > 1$ , we obtain the finite sequence  $\{w^{(k)}\}_{k=1}^K$  of solutions to (16)–(17). Then the Rothe’s function  $w_\tau(x, t)$  is given as the linear interpolant in  $t$

$$w_\tau(x, t) = w^{(k-1)}(x) + \frac{t - t_{k-1}}{\tau} \left( w^{(k)}(x) - w^{(k-1)}(x) \right) \quad \text{for } t_{k-1} \leq t \leq t_k. \tag{18}$$

If  $\Omega$  is a bounded domain with the  $C^{2,\xi}$ -boundary, and  $w \in C^{4,\xi}(\Omega)$ ,  $0 < \xi < 1$ , then for an arbitrary  $T > 0$  and fixed parameters  $0 < \varepsilon < 1$ ,  $0 < \sigma < 1$  the sequence of Rothe’s functions  $\{w_\tau(x, t)\}$  converges uniformly in the  $t$ -variable to the unique classical solution to (13)–(15) as  $\tau \rightarrow 0$ . The proof is similar to that given in [23] and [24] with the very minor changes.

We note that along with the Rothe method, some implicit difference schemes may also be used. However, as observed in numerical experiments, being significantly more complicated to implement, they do not lead to better approximations compared to those obtained by the Rothe method.

Next, we rewrite (16)–17 as

$$-\sum_{i=1}^n \frac{\partial}{\partial x_i} \left( a^{(k-1)} \frac{\partial w^{(k)}}{\partial x_i} \right) + q^{(k-1)}(x) w^{(k)} = F^{(k-1)}(x) \quad \text{in } \Omega_k, \tag{19}$$

$$\nabla w^{(k)} \cdot \nu = 0 \quad \text{on } \partial\Omega_k, \tag{20}$$

where

$$q^{(k)} = \frac{1}{\tau g_\varepsilon^{(k)}}, \quad F^{(k)} = q^{(k)} \left[ w^{(k)} - A^* \left( Aw^{(k)} - v_m \right) \right].$$

Under the conditions indicated above, *a priori* estimate  $|w_\tau(x, t_k)| \leq C_1$ ,  $|\partial_{x_i} w_\tau(x, t_k)| \leq C_2$ , where  $C_1, C_2 > 0$ , takes place for all  $t_k \leq T$ . According to the Schauder’s theory [25, 26], it ensures the unique solvability of the problem (19)–(20).

In the mathematics literature there are available several efficient finite-difference schemes (see, e.g., [27–30]). Without loss of generality, we consider the second order approximation of (19)–(20) in two dimensions. Let  $\bar{\Omega}_k$  be a unit square

$$\bar{\Omega}_k = \{(x_1, x_2) : 0 \leq x_i \leq 1, (i = 1, 2)\}$$

on which we define the uniform grids

$$\begin{aligned} \bar{g} &= \{(x_1, x_2) : x_{1l} = lh, x_{2m} = mh, hN = 1, (l, m = 0, 1, \dots, N)\}, \\ g &= \{(x_1, x_2) : x_{1l} = lh, x_{2m} = mh, hN = 1, (l, m = 1, 2, \dots, N - 1)\}, \end{aligned}$$

so that  $\Gamma = \bar{g} \setminus g$  is the discrete boundary. On  $\bar{g}$  we introduce the grid function  $y = y_{lm}$  and on  $g$  we approximate the differential operator in the left-hand side of the equation (19) as follows

$$\hat{L}y = (s_1 y_{\bar{x}_1})_{x_1} + (s_2 y_{\bar{x}_2})_{x_2}, \tag{21}$$

where

$$\begin{aligned} (s_1 y_{\bar{x}_1})_{x_1} &= \frac{1}{h^2} [(s_1)_{l+1m}(y_{l+1m} - y_{lm}) - (s_1)_{lm}(y_{lm} - y_{l-1m})], \\ (s_2 y_{\bar{x}_2})_{x_2} &= \frac{1}{h^2} [(s_2)_{lm+1}(y_{lm+1} - y_{lm}) - (s_2)_{lm}(y_{lm} - y_{lm-1})], \\ (s_1)_{lm} &= \frac{1}{2} [a(x_{1l-1}, x_{2m}) + a(x_{1l}, x_{2m})], \\ (s_2)_{lm} &= \frac{1}{2} [a(x_{1l}, x_{2m-1}) + a(x_{1l}, x_{2m})]. \end{aligned}$$

Denoting  $\hat{q} = q(x_{1l}, x_{2m})$ ,  $\hat{F} = F(x_{1l}, x_{2m})$ , we arrive to the following difference equation

$$-\hat{L}y + \hat{q}y = \hat{F}, \quad x \in g, \tag{22}$$

subject to the boundary conditions

$$\begin{aligned} -3y_{1m} + 4y_{2m} - y_{3m} &= 0, & \text{for } x_1 = 0, (m = 1, 2, \dots, N - 1), \\ y_{(N-2)m} - 4y_{(N-1)m} + 3y_{Nm} &= 0, & \text{for } x_1 = 1, (m = 1, 2, \dots, N - 1), \\ -3y_{l1} + 4y_{l2} - y_{l3} &= 0, & \text{for } x_2 = 0, (l = 1, 2, \dots, N - 1), \\ y_{l(N-2)} - 4y_{l(N-1)} + 3y_{lN} &= 0, & \text{for } x_2 = 1, (l = 1, 2, \dots, N - 1), \\ -3(y_{10} - y_{01}) + 4(y_{20} + y_{02}) - (y_{30} - y_{03}) &= 0, & l = 0, m = 0, \\ 3(y_{0N} + y_{1N}) - 4(y_{2N} + y_{0(N-1)}) + (y_{3N} + y_{0N}) &= 0, & l = 0, m = N, \\ 6y_{NN} - 4(y_{(N-1)N} + y_{N(N-1)}) + (y_{(N-2)N} + y_{N(N-2)}) &= 0, & l = N, m = N, \\ 3(y_{01} + y_{N0}) - 4(y_{02} + y_{(N-1)0}) + (y_{(N-2)0} - y_{03}) &= 0, & l = N, m = 0. \end{aligned} \tag{23}$$

Note that components of the gradient in (20) are approximated by finite differences with  $O(h^2)$  including the end points. Also, in computations it is convenient to transform (22)–(23) to the Dirichlet difference problem with the homogeneous boundary conditions on an extended grid

$$\bar{g}_{ex} = \{(x_1, x_2) : x_{1l} = lh, x_{2m} = mh, hN = 1, (l, m = -1, 0, 1, \dots, N, N + 1)\}$$

(see, e.g., [31], Chapter 10, item 10.2.4, pp. 252–254). The solution of the difference problem (22)–(23) converges to the classical solution to (19)–(20) in the discrete  $L^2$  and  $W_2^1$  norms. However, it was observed in the numerical



experiments that for the sufficiently small parameters  $\sigma$ ,  $\varepsilon$  and step size  $h$  and for the sufficiently large local variation of  $a^{(k)}$  (a high contrast) a small change in entries of a matrix, which corresponds to (22)–(23), and also in the right-hand side  $\tilde{F}$  may cause a significant change in the numerical solution. In other words, a resulting system of linear algebraic equations is ill-conditioned. Because of this, a Krylov subspace methods, such as Conjugate Gradient (CG) or the alternate-triangular, either do not ensure the convergence or possess extremely low rates of convergence. To overcome these difficulties, some preconditioners were used when solving a corresponding system of linear algebraic equations. There is available in the mathematics literature a variety of preconditioning techniques (see, e.g., surveys in [32, 33]) which ensure the efficient computations at a reasonable cost. In our numerical experiments we have used an implicit version of the Preconditioned Conjugate Gradient (PCG) method (see, e.g., [30]), in which the error of each iteration is minimized in the energy norm, and the correction vector from the Krylov subspace is determined.

**4. Numerical experiments.** In computer simulations a planar domain  $\Omega = (0, 1) \times (0, 1)$  is considered, and a uniform grid is introduced on  $\Omega$ . To simulate the distorted images for the numerical experiments, we exploit a real high resolution abdominal CT-scan of a human, the actual Hounsfield units are rescaled to the density units in the realistic range and then normalized with respect to the maximum value. The resulting image is embedded into the grid and used further as a ground truth image. To simulate the noisy images, we use the simple stochastic model of the additive normally distributed noise with the prescribed level of the relative error ranging from 0.001 to 0.15. The blur is simulated by convolving a Gaussian filter with the ground truth image, so that the filter represents a point-spread function. Since the blur and noise are combined in simulations, the Peak Signal-to-Noise Ratio (PSNR) is exploited as a quality metric for the simulated images

$$\text{PSNR} = 20 \log_{10} \left( \frac{N}{\|\tilde{v} - v\|_2} \right),$$

where  $N = 256$  in the numerical experiments. Note that the PSNR is smaller for the noisy/blurred images and it is larger for the restored images. The ground truth and the sequence of the simulated noisy and blurred images are shown in Figure 1.

It has been observed in the process of numerical experiments that the choice of the weighting function has a significant impact on the reconstruction of high-resolution images. In particular, if  $\alpha = \text{const} > 0$ , then the use of the so-called a priori selection, that is  $\alpha = C\delta^q$ ,  $0 < q < 2$ ,  $1 < C < 2$ , provides edge preserving, though it does not eliminate the staircase effect well and does not compensate for the loss of contrast. Unfortunately, there are still no rigorous criteria for choosing a weighting function  $\alpha = \alpha(x)$ . It is only known that these functions should be large away from edges while they should be small near them. A family of such functions can be constructed by the following heuristic formula

$$\alpha(x) = \frac{1}{1 + C|v_m|^2}, \quad C = \text{const} > 0.$$

In the numerical experiments, a popular in image processing mollifier  $v_m = C|\nabla\Phi * \tilde{v}|^2$  is used along with some other delta-like mollifiers (see, e.g., [34]). Here,  $\Phi$  is the fundamental solution to the two dimension heat equation with the unit thermal diffusivity, in which the scaling parameter  $\lambda = \sqrt{2t}$  is introduced, so that its square can be interpreted as a variance in the Gaussian kernel. We have observed that all such mollifiers provide edge preserving while significantly suppress the staircase effect and loss of contrast.

In the numerical experiments we also observe that the time dependence of the energy functional

$$\int_{\Omega} \alpha(x) |\nabla u^{\sigma\varepsilon}(x, t)| dx$$

is very similar to one obtained for conductivity imaging [35, see Figure 5.3]. This property allows us to select the effective values of  $T \geq 10$ . In the presence of only roundoff errors and beginning with  $T = 50$ , we also observe that the relative error of  $u^{\sigma\varepsilon}$  does not exceed  $1.15 \cdot 10^{-4}$  for  $\sigma, \varepsilon \in (10^{-6}, 10^{-4})$ . Based on this observation, the parameters  $\sigma$  and  $\varepsilon$  have been set up to  $10^{-5}$  in all the numerical experiments.

The computational effectiveness of image denoising and deblurring based on the Approximate Weighted Mean Curvature Flow model (AWMCF) is demonstrated in comparison with the other techniques, such as the VH-Regularization (VHR) [6] and Weighted Total Variation Flow model (WTVF) [36]. Using different definitions of the total variation, these techniques are not equivalent, so that they provide different approximations



Figure 1. The simulated distorted images. From left to right: in the upper row — the ground truth image and the simulated “good” (PSNR=40) image; in the lower row — the simulated “acceptable” (PSNR=25) and “poor” (PSNR=18) images.



Figure 2. The images restored by the VHR. From left to right: in the upper row — the ground truth image and the images denoised/deblurred from the “good” one; in the lower row — the images denoised/deblurred from the “acceptable” and “poor” ones.

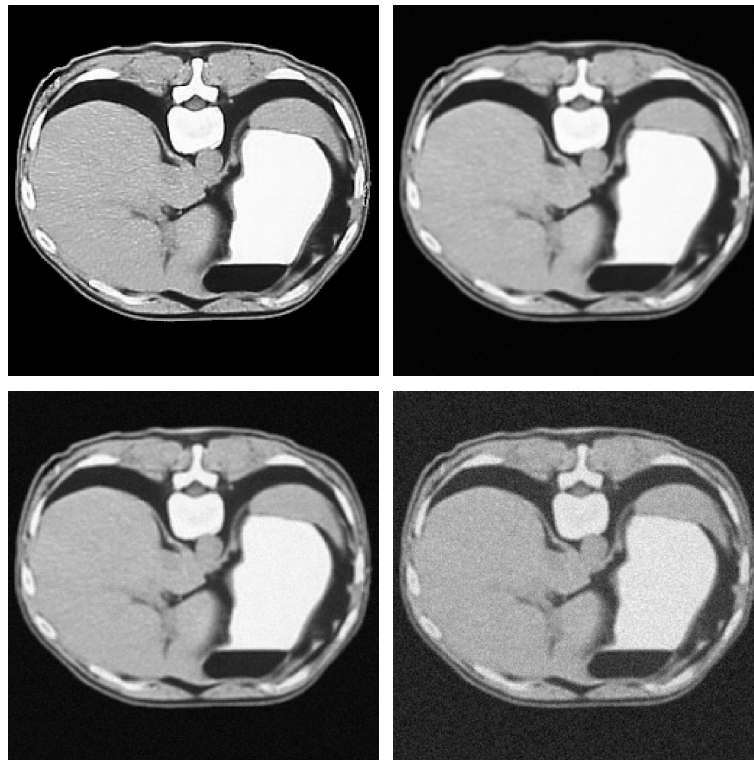


Figure 3. The images restored by the WTVF. From left to right: in the upper row — the ground truth image and the images denoised/deblurred from the “good” one; in the lower row — the images denoised/deblurred from the “acceptable” and “poor” ones.

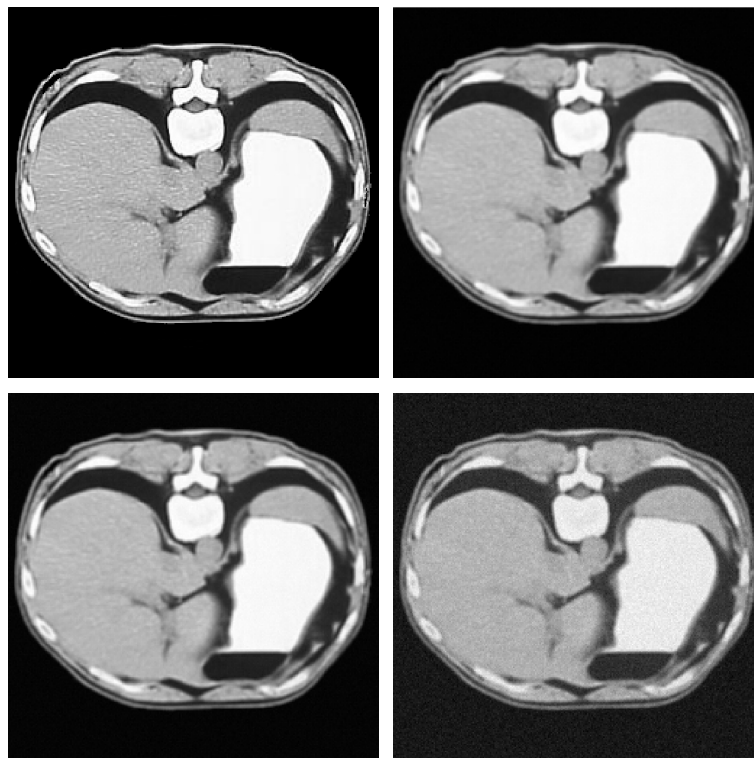


Figure 4. The images restored by the AWMCF. From left to right: in the upper row — the ground truth image and the images denoised/deblurred from the “good” one; in the lower row — the images denoised/deblurred from the “acceptable” and “poor” ones.

of the ground truth solution. Recall that the VHR exploits the Tikhonov regularization with the total VH (Vitalli-Hardy) variation on the class of functions of two variables as a stabilizer, whereas the WTVF model looks similar to (10)–(12) but without the term  $|\nabla u|$  in the right-hand side of (10).

To perform the VHR, in [6] the Conjugate Gradient (CG) method was used together with the homogeneous Dirichlet boundary conditions, and the constant regularization parameter  $\alpha$  was selected by the generalized residual method. To preserve authenticity, we preserve these features for comparison with the WTVF [36] and AWMCF models. The images restored by VHR are shown in Figure 2. We emphasize, however, that if one uses some preconditioners in the CG method and the homogeneous Neumann boundary condition, then the reconstructed images will be comparable in quality to ones reconstructed by WTVF. Unlike the AWMCF model, establishing existence and uniqueness results for the WTVF model does not require the viscosity theory. Also, in contrast to the AWMCF, in the WTVF a semi-implicit difference scheme was used in computations. The images restored by the WTVF are shown in Figure 3. Finally, the images reconstructed by the AWMCF are shown in Figure 4. Along with a visual comparison of denoised/deblurred images, a comparison of the corresponding PSNRs is presented in Table 1.

Table 1. Comparison of the image PSNRs

Images	Good, $\delta = 0.01$	Acceptable, $\delta = 0.05$	Poor, $\delta = 0.10$
Noisy-Blurred	40	25	18
Restored by VHR	45.17	26.39	21.95
Restored by WTVF	47.41	37.52	27.42
Restored by AWMCF	51.49	45.77	31.49

**5. Conclusions.** A new technique has been proposed and numerically implemented for image denoising and deblurring. It is based on the approximate weighted mean curvature flow model that describes motion of the level surface of a flow by the weighted mean curvature. Compared to the known total variation flow models, the proposed one provides better spatial adaptivity, as well as it suppresses the staircase effect and prevents loss of contrast. The numerical studies have been performed with a real CT scan of a human body. The results of image denoising and deblurring obtained by the proposed technique are comparable to the results obtained by the other methods.

## References

1. E. K. Oikonomou, H. W. West, and C. Antoniades, “Cardiac Computed Tomography: Assessment of Coronary Inflammation and Other Plaque Features,” *Arterioscler. Throm. Vasc. Biol.* **39** (11), 2207–2219 (2019). doi 10.1161/ATVBAHA.119.312899.
2. S. Kulcarni, J. A. Rumberger, and S. Jha, “Electron Beam CT: A Historical Review,” *Am. J. Roentgenol.* **216** (5), 1222–1228 (2021). doi 10.2214/AJR.19.22681.
3. I. F. Dorofeev, “On the Solution of Integral Equations of the First Kind in the Class of Functions of Bounded Variation,” *Dokl. Akad. Nauk SSSR* **244** (6), 1303–1307 (1979).
4. A. V. Goncharsky and V. V. Stepanov, “On Uniformly Approximating a Solution of Bounded Variation for Ill-Posed Problems,” *Dokl. Akad. Nauk SSSR* **248** (1), 20–22 (1979).
5. A. S. Leonov, “On the Regularization of Ill-Posed Problems with Discontinuous Solutions and an Application of This Methodology for the Solution of Some Nonlinear Equations,” *Dokl. Akad. Nauk SSSR* **250** (1), 31–35 (1980).
6. A. S. Leonov, “Numerical Piecewise-Uniform Regularization for Two-Dimensional Ill-Posed Problems,” *Inverse Probl.* **15** (5), 1165–1176 (1999). doi 10.1088/0266-5611/15/5/304.
7. L. I. Rudin, S. Osher, and E. Fatemi, “Nonlinear Total Variation Based Noise Removal Algorithms,” *Physica D: Nonlinear Phenomena* **60** (1–4), 259–268 (1992). doi 10.1016/0167-2789(92)90242-F.
8. D. L. Phillips, “A Technique for the Numerical Solution of Certain Integral Equations of the First Kind,” *J. ACM* **9** (1), 84–97 (1962). doi 10.1145/321105.321114.
9. V. K. Ivanov, V. V. Vasin, and V. P. Tanana, *Theory of Linear Ill-Posed Problems and Its Applications* (De Gruyter, Berlin, 2002). doi 10.1515/9783110944822.
10. E. Giusti, *Minimal Surfaces and Functions of Bounded Variation* (Springer, New York, 1984). doi 10.1007/978-1-4684-9486-0.



11. A. Chambolle, “An Algorithm for Total Variation Minimization and Applications,” *J. Math. Imaging Vis.* **20** (1–2), 89–97 (2004). doi [10.1023/B:JMIV.0000011325.36760.1e](https://doi.org/10.1023/B:JMIV.0000011325.36760.1e).
12. W. Ring, “Structural Properties of Solutions to Total Variation Regularization Problems,” *ESAIM: Math. Model. Numer. Anal.* **34** (4), 799–810 (2000). doi [10.1051/m2an:2000104](https://doi.org/10.1051/m2an:2000104).
13. M. Nikolova, “Local Strong Homogeneity of a Regularized Estimator,” *SIAM J. Appl. Math.* **61** (2), 633–658 (2000). doi [10.1137/S0036139997327794](https://doi.org/10.1137/S0036139997327794).
14. L. Vese, “A Study in the BV Space of a Denoising–Deblurring Variational Problem,” *Appl. Math. Optim.* **44** (2), 131–161 (2001). doi [10.1007/s00245-001-0017-7](https://doi.org/10.1007/s00245-001-0017-7).
15. Y. G. Chen, Y. Giga, and S. Goto, “Uniqueness and Existence of Viscosity Solutions of Generalized Mean Curvature Flow Equations,” *J. Differ. Geom.* **33** (3), 749–786 (1991). doi [10.4310/jdg/1214446564](https://doi.org/10.4310/jdg/1214446564).
16. L. C. Evans and J. Spruck, “Motion of Level Sets by Mean Curvature. I,” *J. Differ. Geom.* **33** (3), 635–681 (1991). doi [10.4310/jdg/1214446559](https://doi.org/10.4310/jdg/1214446559).
17. P. Sternberg and W. P. Ziemer, “Generalized Motion by Curvature with a Dirichlet Condition,” *J. Differ. Equ.* **114** (2), 580–600 (1994). doi [10.1006/jdeq.1994.1162](https://doi.org/10.1006/jdeq.1994.1162).
18. A. Lichnerwsky and R. Temam, “Pseudosolutions of the Time-Dependent Minimal Surface Problem,” *J. Differ. Equ.* **30** (3), 340–364 (1978). doi [10.1016/0022-0396\(78\)90005-0](https://doi.org/10.1016/0022-0396(78)90005-0).
19. G. Chavent and K. Kunisch, “Regularization of Linear Least Squares Problems by Total Bounded Variation,” *ESAIM: Control Optim. Calc. Var.* **2**, 359–376 (1997). doi [10.1051/cocv:1997113](https://doi.org/10.1051/cocv:1997113).
20. R. L. Jerrard, A. Moradifam, and A. I. Nachman, “Existence and Uniqueness of Minimizers of General Least Gradient Problems,” *J. Reine Angew. Math.* **2018** (734), 71–97 (2018). doi [10.1515/crelle-2014-0151](https://doi.org/10.1515/crelle-2014-0151).
21. O. A. Ladyzhenskaya, V. A. Solonnikov, and N. N. Uraltseva, *Linear and Quasilinear Equations of Parabolic Type* (Amer. Math. Soc., Providence, 1968).
22. E. Rothe, “Zweidimensionale parabolische Randwertaufgaben als Grenzfall eindimensionaler Randwertaufgaben,” *Math. Annal.* **102**, 650–670 (1930).
23. O. A. Ladyzhenskaya, “Solution of the First Boundary Problem in the Large for Quasi-Linear Parabolic Equations,” *Tr. Mosk. Mat. Obs.* **7**, 149–177 (1958).
24. T. D. Ventzel, “The First Boundary Problem and the Cauchy Problem for Quasi-Linear Parabolic Equations with Several Space Variables,” *Mat. Sb. N. S.* **41** (3), 499–520 (1957).
25. D. Gilbarg and N. S. Trudinger, *Elliptic Partial Differential Equations of Second Order* (Springer, Berlin, 2001). doi [10.1007/978-3-642-61798-0](https://doi.org/10.1007/978-3-642-61798-0).
26. J. Schauder, “Über Lineare Elliptische Differentialgleichungen Zweiter Ordnung,” *Math. Z.* **38** (1), 257–282 (1934). doi [10.1007/BF01170635](https://doi.org/10.1007/BF01170635).
27. J. H. Bramble, B. E. Hubbard, and V. Thomée, “Convergence Estimates for Essentially Positive Type Discrete Dirichlet Problems,” *Math. Comput.* **23** (108), 695–709 (1969).
28. B. S. Jovanović and E. Süli, *Analysis of Finite Difference Schemes for Linear Partial Differential Equations with Generalized Solutions* (Springer, London, 2014). doi [10.1007/978-1-4471-5460-0](https://doi.org/10.1007/978-1-4471-5460-0).
29. A. A. Samarskii, “On the Convergence and Accuracy of Homogeneous Difference Schemes for One-Dimensional and Multidimensional Parabolic Equations,” *USSR Comp. Math. Math. Phys.* **2** (4), 654–696 (1963). doi [10.1016/0041-5553\(63\)90534-2](https://doi.org/10.1016/0041-5553(63)90534-2).
30. A. A. Samarskii, *The Theory of Difference Schemes* (CRC Press, Boca Raton, 2001). doi [10.1201/9780203908518](https://doi.org/10.1201/9780203908518).
31. A. A. Samarskii and E. S. Nikolaev, *Numerical Methods for Grid Equations, Vol. II: Iterative Methods* (Birkhäuser, Basel, 1989). doi [10.1007/978-3-0348-9142-4](https://doi.org/10.1007/978-3-0348-9142-4).
32. M. Benzi and M. Tüma, “A Comparative Study of Sparse Approximate Inverse Preconditioners,” *Appl. Num. Math.* **30** (2–3), 305–340 (1999). doi [10.1016/S0168-9274\(98\)00118-4](https://doi.org/10.1016/S0168-9274(98)00118-4).
33. M. Benzi, “Preconditioning Techniques for Large Linear Systems: A Survey,” *J. Comput. Phys.* **182** (2), 418–477 (2002). doi [10.1006/jcph.2002.7176](https://doi.org/10.1006/jcph.2002.7176).
34. D. A. Murio, *The Mollification Method and the Numerical Solution of Ill-Posed Problems* (Wiley, New York, 1993). doi [10.1002/9781118033210](https://doi.org/10.1002/9781118033210).
35. A. Timonov, “Numerical Solution of a Regularized Weighted Mean Curvature Flow Problem for Electrical Conductivity Imaging,” *SIAM J. Sci. Comput.* **41** (5), B1137–B1154 (2019). doi [10.1137/18M1236071](https://doi.org/10.1137/18M1236071).



36. P. Athavale, R. Xu, P. Radau, et. al, “Multiscale Properties of Weighted Total Variation Flow with Applications to Denoising and Registration,” *Med. Image Anal.*, **23** (1), 28–42 (2015). doi [10.1016/j.media.2015.04.013](https://doi.org/10.1016/j.media.2015.04.013).

*Received*  
*February 16, 2024*

*Accepted for publication*  
*March 10, 2024*

### **Information about the author**

*Alexandre Timonov* – PhD, Professor Emeritus (USA), Senior Scientific Fellow (Russia); 1) St. Petersburg Department of V. A. Steklov Institute of Mathematics of the Russian Academy of Sciences, 27 Fontanka, 191023, St. Petersburg, Russia; 2) University of South Carolina Upstate, University Way, 800, 29303, Spartanburg, USA.